NASA CR-144957

AN ALGORITHM FOR SELECTING A
RADIATION TRANSPORT SUBGRID FOR ABLATION
AND RADIATION COUPLED HYPERSONIC
VISCOUS-SHOCK-LAYER PROBLEMS

By Charles W. Bolz, Jr.

Prepared under Contract No. NAS1-12527 by
COMPUTER SCIENCES CORPORATION
Hampton, Virginia

for

NATIONAL AERONAUTICS AND SPACE ADMINISTRATION

AN ALGORITHM FOR SELECTING A RADIATION

TRANSPORT SUBGRID FOR ABLATION AND RADIATION

COUPLED HYPERSONIC VISCOUS-SHOCK-LAYER PROBLEMS

by

Charles W. Bolz, Jr.

March 1976

SUMMARY

An algorithm is described for selecting a grid subset for calcu-
lating radiative transport. The subset spacing is determined by using
the variation in aerothermal properties across the full grid of the
shock layer. Results show that a radiation grid subset of 15 to 20
points can be used for viscous-shock-layer calculations where approx-
imately 50 grid points are required to define the aerothermal profiles.
Results are presented for various planetary entry conditions with and
without mass injection to lemonstrate both the validity and utility
of the algorithm.

SYMBOLS

C_j mass fraction of species j

$\bar{C}'$ sum of the absolute values of the species concentration mass fraction normal derivatives

e' radiative flux divergence (normal derivative)

m number of radiation grid subset points

$\dot{m}$ nondimensional mass injection rate, $(\rho V)_w / (\rho V)_\infty$

N_{Re} Reynolds number

N number of chemical species

n distance from wall or number of shock-layer grid points

n_s shock standoff distance

T temperature

T' temperature normal derivative

W weighting factor

Z quantity defined by equation 1

Subscripts:

c species concentration

e radiative flux divergence

i,k shock-layer grid index

j species index

ℓ radiation grid subset index

s shock value

t temperature

w wall value

∞ freestream value

Abbreviations:

CWG   course grid near the wall

FWG   fine grid near the wall

INTRODUCTION

Prediction of wall heating and injection rates associated with a hypersonic planetary entry vehicle requires a detailed analysis of thermodynamic and transport processes in the high energy flow field surrounding the vehicle. The most costly part of the analysis is typically the calculation of radiative transport, which may consume 80 to 90 percent of the total computer solution time. Since viscous-shock-layer solution techniques, such as those of Moss (ref. 1), and Anderson and Moss (ref. 2), require 50 to 100 grid points across the shock layer to adequately resolve all significant transport events, computation of radiative transport at all grid points would make these techniques prohibitively expensive for routine usage.

The present report describes an algorithm which uses the variation in aerothermal properties across the shock layer to select a grid subset for computing the radiation transport. Test cases run to validate the algorithm are discussed. Results are presented for Earth and Jupiter entry conditions with moderate to massive injection. To indicate the stability of the algorithm, results are presented for cases in which the full grid does not adequately model important transport events.

PROBLEM

Accurate computation of radiative transport within a high temperature shock layer, such as that experienced by a planetary probe during entry, requires detailed consideration of both continuum and line transitions for ionic, atomic, and molecular species within the layer. Because the strengths of the various transitions are functions of temperature and species concentrations, strong nonlinear couplings can develop between the radiation transport processes, the other shock-layer transport processes, and the mass injection at the wall.

Figures 1 and 2 show the flux divergence and temperature profiles for typical entry cases and illustrate some of the difficulties encountered in selecting a radiation transport grid for the shock layer. The shock layer consists of a weakly viscous outer region of atmospheric species that have been dissociated and partly ionized by the bow shock to form a strongly emitting plasma, a relatively cool injection region near the wall, and a strongly absorbing intermediate viscous mixing layer where the injection species are dissociated by the shock energy. A successful radiation subgrid selection algorithm must identify and properly weight complex events occuring over very small segments of the shock layer.

METHOD

Since radiation transport within the shock layer is dependent primarily upon the temperature and distribution of the constituent species, intuition suggests that the rates of change of these quantities, normal to the wall, should provide sufficient information to define a suitable radiation grid. Numerical experiments indicate that the absolute values of the temperature derivatives and the sum of the absolute values of the species concentration derivatives can be used to identify the spatial regions where the major radiation transport events occur. This is illustrated in figures 1 and 2. For these cases, dissociated injection species form a strongly absorbing region near the wall, which coincides with a peak in the concentration derivative. Large changes in the divergence of the radiation flux within the mixing region are also marked by the concentration derivative. The temperature derivative provides additional information about the mixing layer and its decay marks the transition to the emitting outer layer.

The radiation subgrid is therefore defined by weighting each point of the full shock-layer grid according to the derivatives of temperature, concentration, and, if applicable, the flux divergence computed at the previous iteration. (Including the divergence damps out possible oscillations in the subgrid point selection procedure during the first few iterations of the flow-field solution.) The grid subset is chosen in equal increments of Z, as follows. If

$$Z_k = k + \sum_{i=1}^{k} \left[W_c \frac{\bar{C}'_i}{\bar{C}'_{i,max}} + W_t \frac{|T'|_i}{|T'|_{i,max}} + W_e \frac{|e'|_i}{|e'|_{i,max}} \right] \qquad (1a)$$

6

where

$$\overline{C}'_i = \sum_{j=i}^{N} \left| \frac{\partial C_{i,j}}{\partial n} \right| \qquad (1b)$$

then

$$Z_\ell = \frac{\ell}{m} Z_n \qquad (1 \leq \ell < m) \qquad (2)$$

The method is illustrated in figure 3. To avoid interpolation when $Z_k < Z_\ell < Z_{k+1}$ the subgrid point is chosen to coincide with the point k of the full grid.

The spacing of the radiation subgrid points is controlled by the magnitudes of the weighting factors W. If the weighting factors are set to zero, then $Z = n$, and every $(\frac{n}{m})$ th point will be selected. (For example, if $n = 50$, $m = 10$, every fifth point will be selected.) A high value of W_c will tend to concentrate grid points in spatial regions where the species concentrations are changing rapidly. A high value of W_t will concentrate grid points in the mixing region. A high value of W_e will cluster grid points wherever the flux divergence is rapidly changing.

RESULTS AND DISCUSSION

The radiation grid subset selection procedure defined by equations
1 and 2 and the effects of the weighting factors of equation 1 were
evaluated using the Earth, Venus,and Jupiter entry environments described
in Table I. Cases run included no injection, atmospheric element injection,
coupled ablation, and prescribed ablation injection. For each condition,
a benchmark-case stagnation profile was obtained for fifty points across
the shock layer. The hypersonic viscous-shock-layer program (HYVIS),
which is based on the analysis of references 1 and 2, was used for all
computations. From the resulting chemistry and temperature profiles,the
radiative flux divergence was recomputed for grid subsets of 20, 15 and
10 points and compared with the benchmark results. For each injection
condition, at least one case was run in which the complete stagnation
profile was computed using a radiation grid subset.

Two radiation models were used. Initial testing focused upon Earth
entry using the Engel radiation code (ref. 3) which uses the coupled line-
continuum model of Wilson (ref. 4) to compute the flux divergence directly.
Using a 20 point radiation grid and weighting factors of unity, stagnation
profiles were computed for cases of no injection, air injection,and
coupled-ablation product injection. A local quadratic interpolation
method was used to estimate the flux divergence over the full shock-layer
grid. For ablation cases, all state and transport properties agreed with
benchmark solutions to within 2.5 percent. Cases with no injection and
air injection agreed to within 1.0 percent.

8

Further testing was conducted with the Aerotherm -69 radiation code of Nicolet (ref. 5) which computes the bidirectional radiative flux at each grid point. The HYVIS program computes the divergence by differentiating the net flux profile using a three-point differencing technique. Initial results with the Aerotherm code showed unstable behavior of the flux impinging upon the wall and the flux divergence at both the wall and the shock as the number of points in the radiation grid was reduced. To alleviate this instability, spline interpolation and differentiation for the radiative flux and divergence were tried, and the weighting factors were varied, all without success. The instability was removed by forcing the radiation subgrid to include the two shock layer grid points nearest the wall and two at the shock to "tie down" the ends of the flux divergence curve.

Table II shows results obtained by recomputing the flux divergence for the case of figure 1 with radiation subgrids of 20, 15, and 10 points. Four methods are compared. The basic method used equations 1 and 2 to pick the grid subset and quadratic interpolation and three point differencing to compute the flux divergence. In the second method, spline interpolation and differencing were used. The third method tied down the four end points but used interior subgrid points hand selected by an analyst to represent overall property variation within the layer. (This is equivalent to setting the weighting factors to zero.) For the fourth method the interior subgrid was randomly selected.

For this moderate blowing case, the first three procedures yielded satisfactory results for subgrids down to 15 points. Using 10 points, none of the methods was completely satisfactory. The spline technique

9

performed marginally better in the interior of the layer but did poorly at the end points. This and other cases indicated that use of the local quadratic interpolation scheme with three-point differencing is less likely to cause gross errors if the selection of the subgrid does not adequately model the radiation transport events.

The behavior of the basic method when varying the weighting factors was also investigated. Weighting factors less than 0.5 shifted the subgrid too much towards the shock, thus losing detail in the mixing region. Weighting factors greater than 1.5 concentrated points too heavily around extremum points of the flux divergence profile. Weighting factors of unity were found to be optimum for the cases considered.

Table III shows stagnation profile data for Jovian entry with pre-scribed massive injection. Cases were run for grids which were both course ($\Delta n = 0.02n_S$) and fine ($\Delta n = 0.005n_S$) in the region adjacent to the wall. For each grid a twenty-point radiation subgrid was used to obtain an estimate of the stagnation profile. Then this estimate was used to start the fifty-point solution.

The wall radiative heating was adequately predicted for all the cases, the total spread being less than 5 percent. Considerable discrepancies appear, however, in the flux divergence and the nonradiative (conduction plus convection plus diffusion) heating results. Examination of the temperature and species concentration profiles indicated that the coarse wall grid spacing did not adequately model the absorption layer even with a full radiation grid. With the more appropriate fine wall grid spacing, a twenty-point radiation subgrid adequately modeled the wall radiative heating and flux divergence. The wall nonradiative heating also showed excellent agreement.

10

Cases were also run for Venus entry, with no injection and moderate injection, using radiation subgrids of 20, 15, and 10 points. The trends were very similar to those for earth entry (Table II), so the results are not presented.

CONCLUSIONS

An algorithm is presented for automatically selecting a radiation grid subset based on the variation of aerothermal properties across a shock layer. The method has been tested with two radiation models, three planetary entry conditions, and a wide range of blowing rates. Results presented show that the method yields accurate predictions of radiative transport over a wide range of injection conditions with 15 to 20 subgrid radiation points provided the full grid (50 points), adequately models the major transport processes. Since the cost of performing the radiative calculation is almost directly proportional to the number of grid points, the present algorithm provides a means for substantially reducing the computational cost for calculating radiative flow fields.

REFERENCES

1. Moss, James N., "Reacting Viscous-Shock-Layer Solutions With Multicomponent Diffusion and Mass Injection," TR-411, 1974, NASA.

2. Anderson, E. C., and Moss, J. N., "Numerical Solution of the Hypersonic Viscous-Shock-Layer Equations for Laminar, Transitional and Turbulent Flows of a Perfect Gas over Blunt Axially Symmetric Bodies," TN D-7865, 1975, NASA.

3. Engel, C. D., Farmer, R. C., and Pike, R. W., "Ablation and Radiation Coupled Viscous Hypersonic Shock Layers," CR-112306, 1971, NASA.

4. Wilson, K. H., "Stagnation Point Analysis of Coupled Viscous Radiating Flow with Massive Blowing," CR-1548, 1970, NASA.

5. Nicolet, W. E., "Advanced Methods for Calculating Radiation Transport in Ablation Product Contaminated Boundary Layers," CR-1656, 1970, NASA.

TABLE I.-PLANETARY ENTRY CONDITIONS FOR
RADIATION SUBGRID TEST CASES

Properties	Earth	Venus	Jupiter
Altitude, km	62.200	83.300	108.200
Velocity, km/sec	15.200	8.780	40.000
Mach number	43.000	43.400	47.500
Temperature, k	250.000	180.000	145.000
Density, g/cm^3	2.340×10^{-7}	5.79×10^{-6}	6.900×10^{-7}
Nose radius, m	0.305	0.339	0.229
Atmospheric Composition, Mass Fractions	0.76 N_2 0.24 O_2	1.00 CO_2	0.74 H_2 0.26 He
Injectant Composition, Mass Fractions	0.147 O 0.050 N 0.730 C 0.073 H	0.110 O 0.004 N 0.851 C 0.035 H	1.00 C
$\dot{m} = (\rho V)_w / (\rho V)_\infty$	0.0-0.125	0.0-0.2	0.0-0.4

TABLE II.-COMPARISON OF RADIATION SUBGRID MODELS

	Flux at Wall MW/m²	Divergence at Wall, GW/m³	Divergence Minimum, GW/m³	Divergence at Shock, GW/m³
Baseline (50 points)	8.43	-1.259	-1.707	23.47
Basic Method:				
20 points	8.26	-1.239	-1.679	23.54
15 points	8.32	-1.254	-1.668	23.37
10 points	8.25	-1.336	-1.534	22.72
Splines:				
50 points	8.43	-1.223	-1.720	21.40
20 points	8.23	-1.215	-1.693	20.30
15 points	8.11	-1.227	-1.710	19.88
10 points	7.91	-1.210	-1.656	19.98
Hand Selected				
20 points	8.25	-1.254	-1.698	23.49
15 points	8.30	-1.264	-1.686	23.37
10 points	8.32	-1.327	-1.482	11.75
Random Grid				
20 points	8.24	-1.223	-1.576	23.76
15 points	8.13	-1.191	-1.524	23.79
10 points	7.75	-1.037	-0.991	24.33

15

TABLE III.-JOVIAN ENTRY WITH PRESCRIBED INJECTION

$$(N_{Re} = 1.34\times10^6, \quad p = 9.86 \text{ atm}, \quad \dot{m} = 0.40)$$

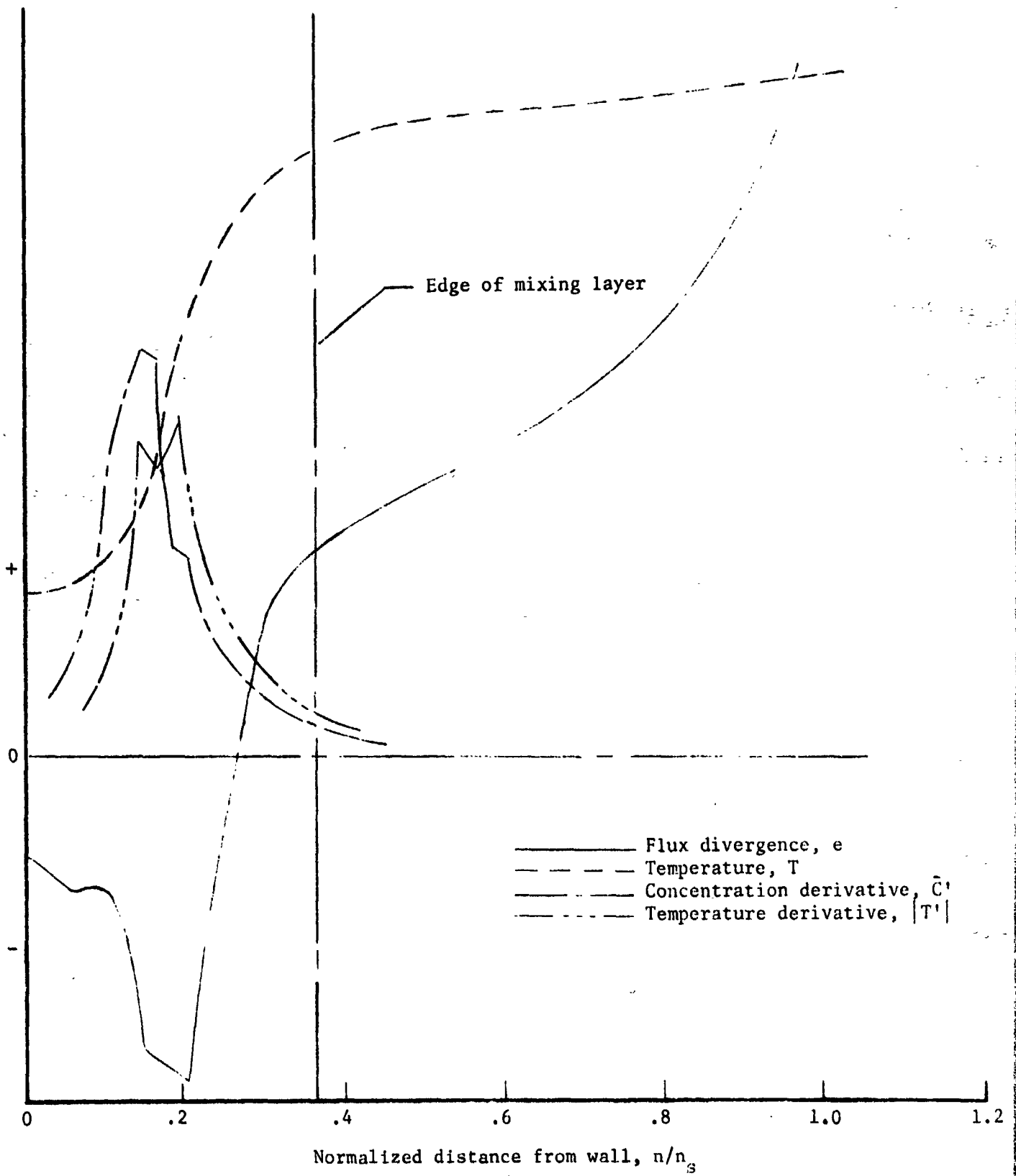| CASE	CWG-50	CWG-20	FWG-50	FWG-20
Grid Points	50	20	50	20
Wall Mesh	Coarse	Coarse	fine	fine
Shock Standoff, m	0.01896	0.01719	0.01877	0.01390
Wall radiative heating, Mw/m2				
Continuum	191.4	188.8	194.2	192.3
Line	58.8	61.0	64.7	69.9
Total	250.1	249.8	258.9	262.2
Flux Divergences, TW/m3				
Wall	-39	-10	-65	-62
$0.05*n_s$	-257	-201	-290	-291
$0.88*n_s$	113	112	116	113
$1.00*n_s$	403	407	503	500
Wall nonradiative heating, MW/m	-2.320	-4.073	0.908	0.849

Figure 1. - Radiative flux divergence and other selected
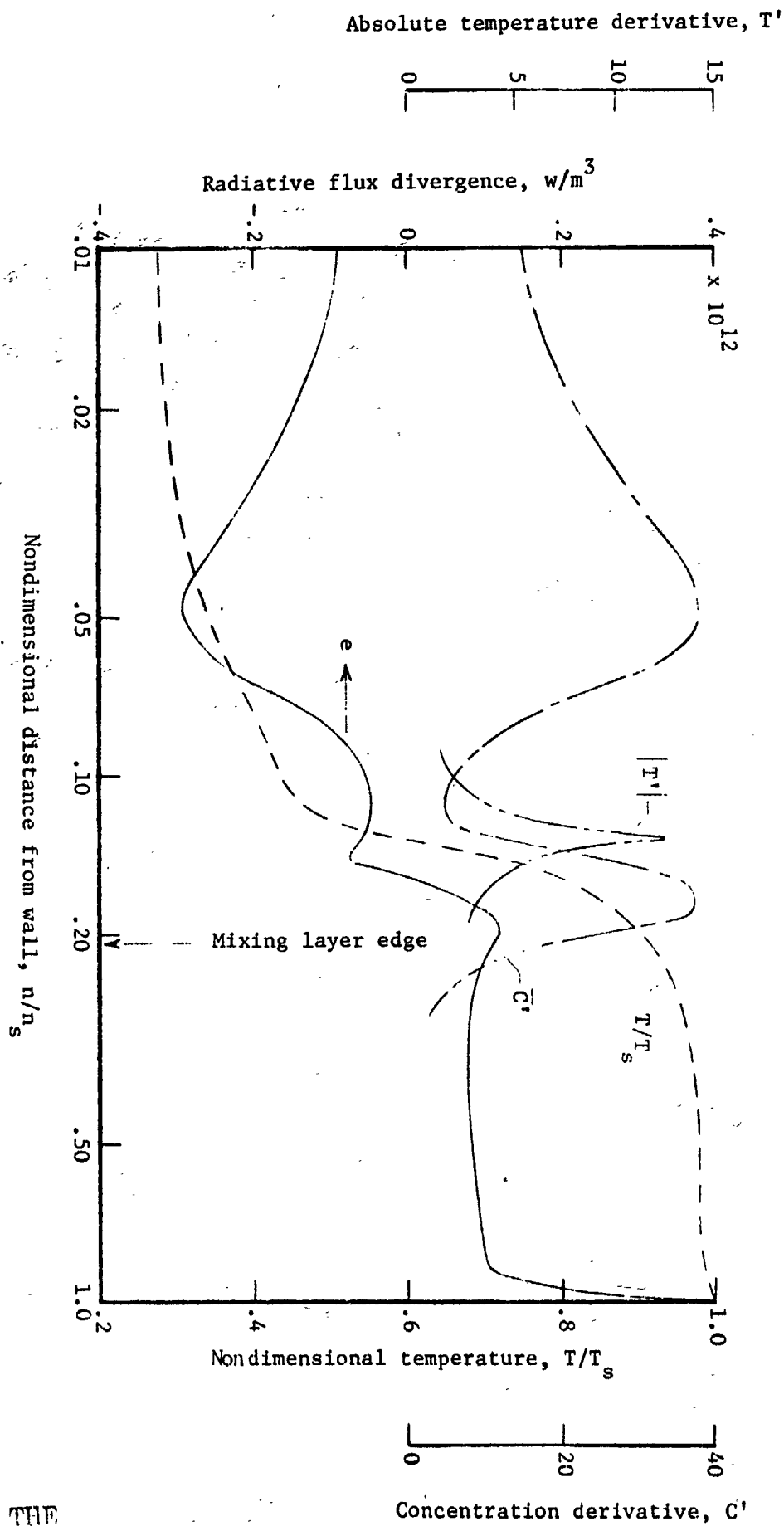shock-layer properties (Earth entry typical).

Figure 2. – Radiative flux divergence and other selected shock-layer properties (Jovian entry, ṁ = 0.42).

$$Z_n = n + \sum_{i=1}^{n} f(\overline{C}'_i, T'_i, e_i)$$

$$Z_{k+1} = (k+1) + \sum_{i=1}^{k+1} f(\overline{C}'_i, T'_i, e_i)$$

$$Z_\ell = \frac{\ell}{m} \cdot Z(n)*$$

$$Z_k = k + \sum_{i=1}^{k} f(\overline{C}'_i, T'_i, e_i)$$

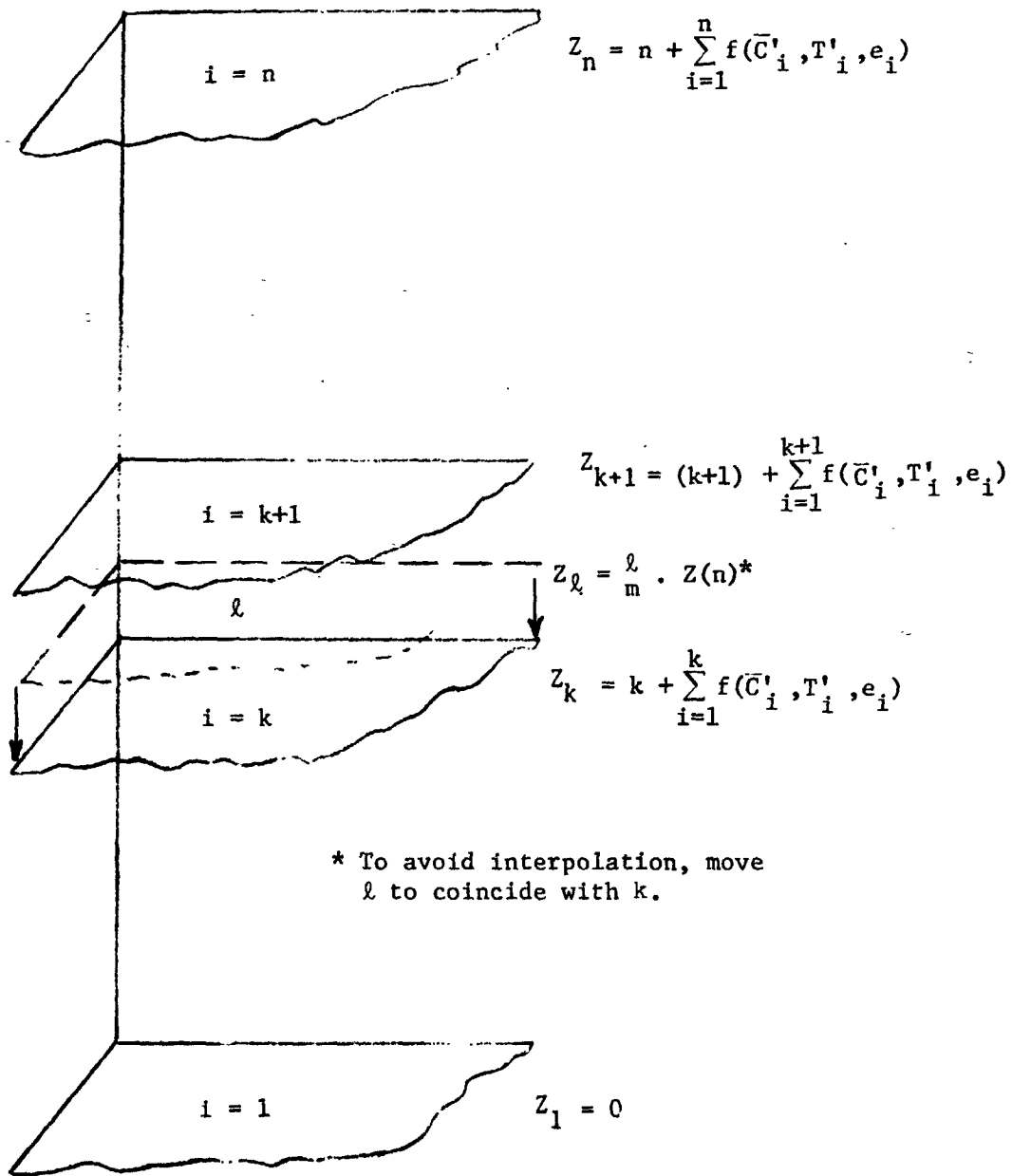* To avoid interpolation, move ℓ to coincide with k.

$$Z_1 = 0$$

Figure 3. - Radiation subgrid selection procedure.